Optics Letters

1.2 W single-frequency Tm^{3+}/Ho^{3+} co-doped fiber oscillator at 2050 nm

Chaodu Shi,[1,2,†] Peiheng Jiang,[1,2,†] Shijie Fu,[1,2,*] Quan Sheng,[1,2] Lin Chen,[3] Wei Shi,[1,2,4] Cailing Fu,[3,5] Yiping Wang,[3] and Jianquan Yao[1,2]

[1]School of Precision Instrument and Optoelectronics Engineering, Tianjin University, Tianjin 300072, China
[2]Key Laboratory of Optoelectronic Information Technology (Ministry of Education), Tianjin University, Tianjin 300072, China
[3]Key Laboratory of Optoelectronic Devices and Systems of Ministry of Education and Guangdong Province, College of Physics and Optoelectronics Engineering, Shenzhen University, 518060, China
[4]shiwei@tju.edu.cn
[5]fucailing@szu.edu.cn
[†]These authors contributed equally to this Letter.
[*]shijie_fu@tju.edu.cn

Received 7 August 2023; revised 18 October 2023; accepted 26 October 2023; posted 26 October 2023; published 20 November 2023

In this Letter, a watt-level single-frequency fiber oscillator at 2050 nm was demonstrated for the first time, to the best of our knowlegde, in a linear laser cavity with a piece of an un-pumped Tm^{3+}/Ho^{3+} co-doped fiber serving as a saturable absorber. With delicate optimization of mode filtering effect of the dynamic gratings formed in the saturable absorber, a maximum single-frequency laser output power of 1.2 W was achieved under a total bidirectional pump power of 5.8 W at 1570 nm, and the corresponding optical efficiency is 20.7%. This is, to the best of our knowledge, the highest power of a single-frequency fiber oscillator at the wavelength above 2 μm.

https://doi.org/10.1364/OL.502554

Single-frequency fiber lasers operating at the wavelength region above 2 μm have attracted lots of attention due to their widespread applications on free-space optical communication, high-resolution spectroscopy, and coherent Doppler LIDAR [1–3]. Tm^{3+}-doped fiber (TDF) has been widely used to achieve single-frequency laser operation around 2.0 μm [4–10], and a maximum output power of 0.9 W at 1978.6 nm has been demonstrated from a ring cavity with a silica prolate microresonator as an ultranarrow bandwidth filter [4]. However, the diminished emission cross section of Tm^{3+} at a longer wavelength restrains the power level of single-frequency Tm^{3+}-doped fiber lasers above 2 μm [8,9]. Up to now, the highest single-frequency laser power of 215 mW at 2050 nm was demonstrated by Zhang *et al.* in 2022, where a ring laser cavity was employed with 5 m of TDF as the gain media [10].

Actually, in this wavelength regime, Ho^{3+}-doped fiber (HDF) exhibits a broad emission spectrum from 1.95 μm to 2.2 μm, and the emission peak locates around 2050 nm, which facilitates laser operation at a longer wavelength compared with TDF [11,12]. However, the two main absorption peaks of Ho^{3+}, at 1.15 μm and 1.95 μm, respectively [13,14], cannot be covered by commercial high-power laser diodes that Ho^{3+}-doped fiber lasers are generally pumped by Yb^{3+}- or Tm^{3+}-doped fiber lasers. In 2009, Wu *et al.* reported a single-frequency distributed Bragg reflection (DBR) Ho^{3+}-doped fiber laser [15], in which 2-cm-long heavily Ho^{3+}-doped germanate fiber (3 wt.% Ho_2O_3 doping concentration) was in-band pumped by a 1950 nm Tm^{3+}-doped fiber laser. A maximum output power of 60 mW was achieved at 2053 nm with a pump power of 800 mW. In 2019, Wolf *et al.* presented a single-frequency distributed feedback (DFB) Ho^{3+}-doped fiber laser, in which 42-mm-long π-phase-shifted grating was directly inscribed in the Ho^{3+}-doped silica fiber and pumped by a 1125 nm Yb^{3+}-doped fiber laser [16]. Due to the low pump absorption coefficient of the active fiber at 1125 nm (about 45 dB/m), only 53 mW single-frequency laser output at 2070 nm was obtained under a pump power of 5.2 W. In singly Ho^{3+}-doped fiber, clustering-associated inhomogeneous energy transfer upconversion and cross relaxation significantly constrain the laser efficiency [17]. Moreover, the short laser cavity with a DBR and DFB structure also limits the single-frequency Ho^{3+}-doped fiber laser to a power level of tens of milliwatt.

The Tm^{3+}/Ho^{3+} co-doped fiber (THDF) has been developed as another gain medium to achieve fiber lasers above 2 μm [18], where Tm^{3+} serves as a sensitizer and the energy transfer from level $^3F_4$ of Tm^{3+} to level $^5I_7$ of Ho^{3+} allows for lasing above 2 μm through the transition $^5I_7 \rightarrow {}^5I_8$ of Ho^{3+}. Thanks to the introduction of Tm^{3+}, the Tm^{3+}/Ho^{3+} co-doped fiber laser can be pumped by a fiber laser at 1570 nm or high-power diode laser at 793 nm [19–21], by which a hundred-watt laser output above 2 μm has been realized [22,23]. In this paper, a watt-level single-frequency fiber laser at 2048.7 nm was demonstrated with a linear cavity structure. Two pieces of THDFs were used in the laser cavity, in which one of them served as the gain medium and was bidirectionally pumped by two 1570 nm fiber lasers and the other one functioned as a saturable absorber (SA) for longitudinal-mode selection.

Generally, in a linear cavity, a spatial hole burning (SHB) effect imposes a restriction on single-longitudinal-mode (SLM)

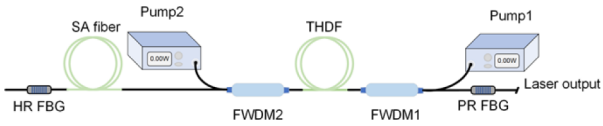

Fig. 1. Schematic of the watt-level 2050 nm single-frequency Tm^{3+}/Ho^{3+} co-doped fiber laser. FBG, fiber Bragg grating; FWDM, filter-type wavelength-division multiplexer; SA, saturable absorber.

laser operation. In addition, limited by the Ho^{3+} ion doping capability in silica glass, long THDF needed for sufficient laser gain increases the linear cavity length and thus decreases the longitudinal-mode spacing, which exacerbates the difficulty on the realization of single-frequency laser. This Letter demonstrates the feasibility of utilizing a linear cavity for high-power single-frequency fiber laser generation with proper selection of the rare-earth-doped fiber-based SA. A maximum single-frequency power of 1.2 W was obtained at 2048.7 nm with a launched 1570 nm pump power of 5.8 W, which is, to the best of our knowledge, the highest power of a single-frequency fiber oscillator above 2 μm. The dynamics of optical spectra and longitudinal mode were also investigated and analyzed for this bidirectionally pumped fiber laser.

The experimental setup of the single-frequency Tm^{3+}/Ho^{3+} co-doped fiber laser is shown in Fig. 1. A 4.6-m single-mode THDF (Coractive, TH512, absorption coefficient at 793 nm is 202 dB/m), which exhibits an absorption coefficient of 43 dB/m at 1570 nm, was used as a gain fiber for laser generation at 2050 nm. The THDF fiber was bidirectionally core-pumped by two 1570 nm fiber lasers. The backward pump source (marked as Pump1) and the forward pump source (marked as Pump2) can provide a maximum output power of 3.1 W and 2.7 W, respectively. The pump lasers were coupled into the gain fiber through the common port of two 1570/2000 nm filter-type wavelength-division multiplexers (named as FWDM1 and FWDM2), respectively. A pair of homemade fiber Bragg gratings (FBGs) was connected to the signal port of these two FWDMs to serve as cavity mirrors. The high-reflectivity (HR) FBG centered at 2048.8 nm has a reflectivity of >99.5% and a 3-dB bandwidth of 0.35 nm, while the partial-reflectivity (PR) FBG centered at 2048.7 nm has a reflectivity of 39.7% and a 3-dB bandwidth of 0.07 nm. To achieve a single-frequency laser operation, another piece of un-pumped THDF was spliced between HR FBG and FWDM2 to work as an SA-based mode selector [24,25]. The length of SA was optimized for stable SLM operation at a high power level. Due to the existence of Ho^{3+}, efficient signal absorption in the THDF-based SA facilitates the formation of a self-tracking dynamic grating that its superior capability on longitudinal-mode selection guarantees stable single-frequency laser operation under a high output power. The total insertion loss of this cavity was around 1.8 dB.

The laser output power of the 2050 nm linear cavity fiber laser was measured as a function of pump power and is shown in Fig. 2. The Pump1 in a backward direction was first launched into the laser through FWDM1, and a laser threshold of 0.7 W was obtained. The laser power increased linearly with a slope efficiency of 18.1%, and an output power of 455 mW was achieved at a maximum pump power of 3.1 W. Then, Pump2 in a forward direction was employed for further laser power increment. An increased slope efficiency of 27.6% resulted in a maximum output power of 1.2 W obtained at the forward pump power of

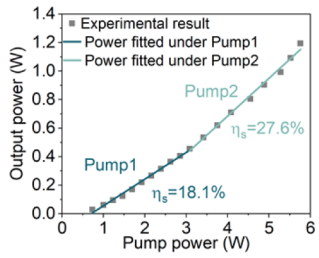

Fig. 2. Measured output power of the 2050 nm THDF laser as a function of 1570 nm pump power.

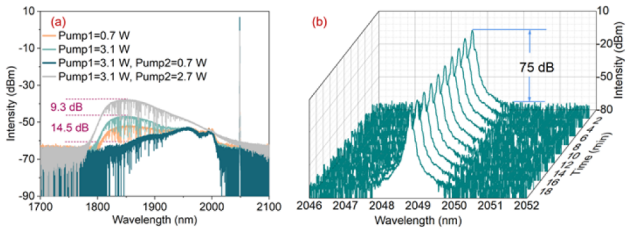

Fig. 3. (a) Optical spectrum evolution of the $Tm^{3\pm}/Ho^{3\pm}$ co-doped fiber laser as a function of pump power measured in a wavelength range of 1700–2100 nm. (b) Measured optical spectra at the maximum output power of 1.2 W in 20 min.

2.7 W (total pump power of 5.8 W). The corresponding optical efficiency was around 20.7%.

The laser spectra under different pump power were measured by an optical spectrum analyzer (OSA, Yokogawa, AQ6375) with a resolution of 0.05 nm and are shown in Fig. 3(a). At a threshold pump power of 0.7 W, severe amplified spontaneous emission (ASE) ranging from 1770 nm to 2000 nm can be observed, which corresponds to the emission spectrum of Tm^{3+} through energy-level transition from $^3F_4$ to $^3H_6$. It indicates that insufficient energy transfer from $^3F_4$ of Tm^{3+} to $^5I_7$ of Ho^{3+} occurs at a low pump power [26], resulting in a low optical signal-to-noise ratio (OSNR) of 38 dB. With the power increase of Pump1, improved energy transfer from Tm^{3+} to Ho^{3+} can be obtained due to the accumulation of population at $^3F_4$ of Tm^{3+}, which induces the intensity decrease of ASE. When the launched power of Pump1 increased to 3.1 W, the ASE intensity at 1850 nm decreased around 9.3 dB, while the ASE ranging from 1950 nm to 2000 nm, which is generated through energy transfer from $^5I_7$ to $^5I_8$ of Ho^{3+}, was detected.

At a maximum pump power, the dominant ASE component stems from Ho^{3+}, and the ASE originating from Tm^{3+} is barely observed that results in an OSNR of 60 dB. This phenomenon manifests that most of the population at $^3F_4$ of Tm^{3+} is transferred to $^5I_7$ of Ho^{3+} instead of $^3H_6$ of Tm^{3+}, and thus the slope efficiency of laser power increases from 18.1% to 27.6% as shown in Fig. 2. Figure 3(b) shows the laser spectra at a maximum output power of 1.2 W in 20 min, which were measured with an OSA resolution of 0.05 nm in a wavelength range from 2046 nm to 2052 nm. An OSNR of 75 dB can be obtained, and the laser central wavelength can be maintained well within the resolution of OSA. A laser with such high OSNR can be further achieved with a long-pass filter to remove the ASE part at the shorter wavelength region.

The longitudinal-mode characteristics of the 2050 nm fiber laser were analyzed by measuring the RF spectrum with an

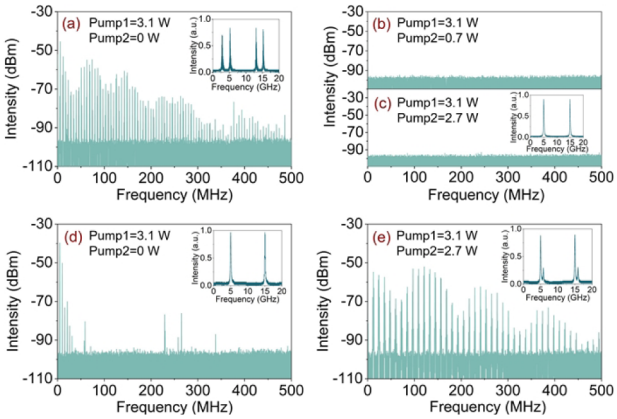

Fig. 4. Measured RF spectra and transmission spectra of scanning FPI of the 2050 nm fiber laser with 11.3 m THDF-based SA at a total pump power of (a) 3.1 W, (b) 3.8 W, and (c) 5.8 W, with 1.5 m TDF-based SA at a total pump power of (d) 3.1 W and (e) 5.8 W.

electrical spectrum analyzer (ESA, Agilent, PXA N9030A) and oscilloscope trace of a scanning Fabry–Perot interferometer (FPI) (Thorlabs, SA210-12B). Figures 4(a) and 4(b) show the measured RF spectra of the laser at a pump power of 3.1 W and 5.8 W, respectively. The resolution bandwidth (RBW) of the ESA was set as 10 kHz. While a longer SA brings a narrower bandwidth of the self-tracking dynamic grating, which is favorable for SLM operation, it also increases the overall length of the laser cavity and reduces the free spectral range (FSR). To achieve high SLM laser output power, the length of THDF-based SA was optimized to 11.3 m experimentally, and thus the cavity length is around 18 m, corresponding to an FSR of 5.7 MHz. Figure 4(a) shows the measured RF spectrum (ranging from 0 MHz to 500 MHz) at 3.1 W of Pump1 power. Beat frequency peaks can be observed from the RF spectrum with a frequency interval corresponding to the FSR of the laser cavity. The oscilloscope trace of FPI, as shown in the inset of Fig. 4(a), also confirms that multi-longitudinal-mode lasing was achieved at this power level. Once the Pump2 power was launched into the gain fiber, the intensity of beat frequency peaks was decreased, and the frequency interval in RF spectrum was enlarged, which indicates that the oscillating longitudinal modes were gradually suppressed with the introduction of Pump2. Finally, SLM operation was achieved as the power of Pump2 increased to 0.7 W, where the laser output power was 620 mW. No beat frequency signal was observed from the measured RF spectrum, as shown in Fig. 4(b). Stable SLM operation can be well maintained as the further increase of pump power; eventually, the single-frequency laser with an output power of 1.2 W was obtained at 2050 nm with the measured RF spectrum properties shown in Fig. 4(c), and SLM operation was further confirmed by the scanning FPI.

The achievement of SLM operation of the laser demonstrated in this Letter is attributed to the employment of SA, where a narrow bandwidth self-tracking dynamic grating was built up through the SHB effect. The dynamic grating is constituted by a refractive index grating (phase grating, RIG) and an absorption grating (amplitude grating) [27,28]. Since the bandwidth of RIG, decided by the length of SA, should be narrower than that of the FSR of the laser cavity for SLM laser operation, the length of SA was optimized in experiment to achieve a high-power single-frequency laser. The theoretical bandwidth of RIG

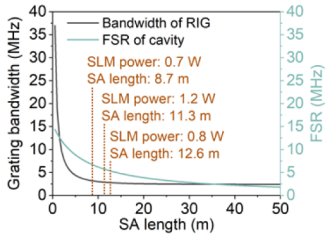

Fig. 5. Theoretical bandwidth of RIG in SA and FSR of laser cavity in relationship with SA length (the experimental results on the maximum achievable SLM laser power at different SA lengths are marked in gold).

[29] and laser cavity FSR are calculated and shown in Fig. 5. Although the SA length allowing for SLM operation can be adjusted in a range of 1.5 m to 35.7 m theoretically, single-frequency laser cannot be obtained in experiment until the SA length was increased to 8.7 m. As shown in Fig. 3(a), severe ASE was generated at a low pump power, which disrupts the refractive index modulation in the SA. As a result, the RIG cannot function well for longitudinal-mode selection, especially for a short piece of SA. With the ASE intensity decrease and laser power increment at a high pump power, the SHB effect for the signal was significantly enhanced in SA, which is beneficial for the formation of a self-tracking dynamic grating and the achievement of single-frequency laser operation. However, it should be noted that too high laser power would wash out the dynamic grating in SA due to the absorption saturation effect [30], especially at the position close to the gain fiber in our experimental setup. Thus the effective length of the dynamic grating would be decreased significantly that deteriorates the bandwidth of the RIG. Therefore, increasing the SA length is necessary to realize high-power SLM laser operation. In our experiment, the achievable single-frequency laser power gradually increased from 0.7 W to 1.2 W when the length of the THDF-based SA increased from 8.7 m to 11.3 m. However, further increase of the SA length to 12.6 m only achieved a single-frequency laser power of 0.8 W. The decreased SLM laser power is mainly attributed to that higher signal absorption in longer SA results in amplitude reduction of the self-tracking dynamic grating, and in turn, the mode-selection capability is weakened. Therefore, the SA length should be properly optimized in consideration of the optical spectrum purity and the signal absorption strength for high-power single-frequency laser generation.

On the other hand, in order to clarify the specific effect of Ho^{3+} in the THDF-based SA on longitudinal-mode selection of the demonstrated 2050 nm single-frequency fiber laser, 1.5 m TDF (Coherent, SM-TDF-10/130-M) was also used as a replaced SA in the experimental setup to characterize the laser longitudinal-mode properties for comparison. It should be pointed out that the length of the TDF was selected to possess the same pump absorption at 1570 nm with that of THDF-based SA. In the controlled experiment, single-frequency laser operation can be only obtained at the laser power below 115 mW, where the pump power was around 1 W. Further increase of pump power induced the instability of single-longitudinal-mode laser operation, and beat frequency peaks can be observed in RF spectrum as shown in Fig. 4(c). RF beat frequencies with an interval of 12 MHz, which corresponds to the cavity FSR, can be found in Fig. 4(d), indicating multi-longitudinal-mode lasing

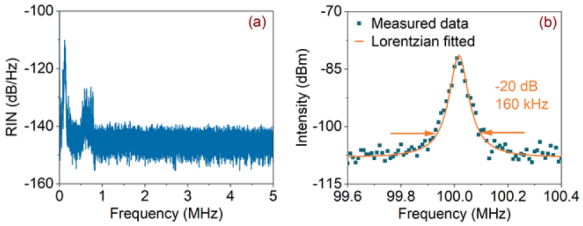

Fig. 6. (a) Measured RIN of the 2050 nm single-frequency fiber laser in a frequency range of 0–5 MHz at the maximum output power of 1.2 W. (b) Measured laser linewidth using the delayed self-heterodyne method and fitted with Lorentzian line shape.

at a maximum pump power of 5.8 W. Therefore, introducing Ho^{3+} to the SA in our demonstration enhances the intensity of the dynamic grating in SA and improves the mode selection capability for higher laser power with single-longitudinal-mode operation [31], owing to the higher absorption cross section of Ho^{3+} at a signal wavelength of 2050 nm.

The relative intensity noise (RIN) of the demonstrated single-frequency laser at a maximum output power of 1.2 W was measured using a photodetector (EOT, ET-5000F) and an ESA with an RBW of 1 kHz, and the result in a frequency range of 0–5 MHz is shown in Fig. 6(a). A relaxation oscillation peak can be observed at 0.12 MHz with an intensity of −110 dB/Hz. As the frequency increases, the RIN intensity decreases rapidly and is stabilized to a level of −152 dB/Hz at the frequency above 1 MHz. It should be noted that the intensity peaks around 0.7 MHz as shown in Fig. 6(a) mainly originate from the electrical noise of DC power supply in the measurement system. The spectral linewidth of the 1.2 W single-frequency laser was measured via a delayed self-heterodyne system with a resolution of 5 kHz and is shown in Fig. 6(b) with a fitted Lorentzian line shape. The measured −20 dB spectral linewidth was found to be 160 kHz, corresponding to a laser linewidth of 8 kHz.

In conclusion, a 1.2 W single-frequency fiber oscillator at 2050 nm was realized with a linear cavity structure, which is, to the best of our knowledge, the first demonstration of a watt-level single-frequency fiber laser at the wavelength above 2 μm. At the maximum laser output power, the laser OSNR was higher than 60 dB considering the ASE component, and the laser linewidth is measured to be around 8 kHz. Our experiment demonstrates that the narrowband filtering effect of the active fiber-based SA is strongly affected by laser optical spectrum purity and signal absorption intensity in SA, which manifests the importance of proper selection of the parameters of the SA, such as signal absorption coefficient, fiber length, etc., for high-power single-frequency laser generation.

Funding. National Natural Science Foundation of China (61975146, 62075159, 62105240, 62275190); Seed Foundation of Tianjin University (2023XPD-0020); Key Technology Research and Development Program of Shandong (2020CXGC010104, 2021CXGC010202).

Disclosures. The authors declare no conflicts of interest.

Data availability. Data underlying the results presented in this paper are not publicly available at this time but may be obtained from the authors upon reasonable request.

REFERENCES

1. T. Wu, X. Peng, W. Gong, Y. Zhan, Z. Lin, B. Luo, and H. Guo, Opt. Lett. **38**, 986 (2013).
2. S. Kameyama, T. Ando, K. Asaka, Y. Hirano, and S. Wadaka, Appl. Opt. **46**, 1953 (2007).
3. Q. Qin, T. Li, F. Yan, T. Feng, W. Sun, W. Han, D. Yang, X. Wang, C. Yu, P. Wang, D. Cheng, Y. Guo, Y. Liu, Y. Jiang, K. Kumamoto, H. Zhou, and Y. Suo, J. Lightwave Technol. **41**, 5275 (2023).
4. J. Zhang, W. Yao, H. Wang, W. Zhou, X. Wu, and S. Shen, IEEE Photonics Technol. Lett. **31**, 1241 (2019).
5. X. Guan, C. Yang, T. Qiao, W. Lin, Q. Zhao, G. Tang, G. Qian, Q. Qian, Z. Yang, and S. Xu, Opt. Express **26**, 6817 (2018).
6. T. Yin, Y. Song, X. Jiang, F. Chen, and S. He, Opt. Express **27**, 15794 (2019).
7. S. Fu, W. Shi, J. Lin, Q. Fang, Q. Sheng, H. Zhang, J. Wen, and J. Yao, Opt. Lett. **40**, 5283 (2015).
8. S. Fu, W. Shi, Y. Feng, L. Zhang, Z. Yang, S. Xu, X. Zhu, R. A. Norwood, and N. Peyghambarian, J. Opt. Soc. Am. B **34**, A49 (2017).
9. C. Shi, S. Fu, G. Shi, S. Sun, Q. Sheng, W. Shi, and J. Yao, Optik **187**, 291 (2019).
10. L. Zhang, Q. Sheng, L. Chen, J. Zhang, S. Fu, Q. Fang, Y. Wang, W. Shi, and J. Yao, Opt. Lett. **47**, 3964 (2022).
11. R. E. Tench, C. Romano, G. M. Williams, J. M. Delavaux, T. Robin, B. Cadier, and A. Laurent, J. Lightwave Technol. **37**, 1434 (2019).
12. B. Beaumont, P. Bourdon, A. Barnini, L. Kervella, T. Robin, and J. Le Gouët, J. Lightwave Technol. **40**, 6480 (2022).
13. R. E. Tench, W. Walasik, and J. M. Delavaux, J. Lightwave Technol. **39**, 3546 (2021).
14. C. Huang, Y. Tang, S. Wang, R. Zhang, J. Zheng, and J. Xu, J. Lightwave Technol. **30**, 3235 (2012).
15. J. Wu, Z. Yao, J. Zong, A. C. Pirson, N. Peyghambarian, and J. Yu, Proc. SPIE **7195**, 71951K (2009).
16. A. A. Wolf, M. I. Skvortsov, V. A. Kamynin, I. V. Zhluktova, S. R. Abdullina, A. V. Dostovalov, V. B. Tsvetkov, and S. A. Babin, Opt. Lett. **44**, 3781 (2019).
17. J. Wang, D. Yeom, N. Simakov, A. Hemming, A. Carter, S. B. Lee, and K. Lee, J. Lightwave Technol. **36**, 5863 (2018).
18. K. Oh, T. F. Morse, A. Kilian, L. Reinhart, and P. M. Weber, Opt. Lett. **19**, 278 (1994).
19. A. Hemming, S. Bennetts, N. Simakov, A. Davidson, J. Haub, and A. Carter, Opt. Express **21**, 4560 (2013).
20. P. Kuan, X. Fan, X. Li, D. Li, K. Li, L. Zhang, C. Yu, and L. Hu, Opt. Lett. **41**, 2899 (2016).
21. S. D. Jackson, A. Sabella, A. Hemming, S. Bennetts, and D. G. Lancaster, Opt. Lett. **32**, 241 (2007).
22. A. Motard, C. Louot, T. Robin, B. Cadier, I. Manek-Hönninger, N. Dalloz, and A. Hildenbrand-Dhollande, Opt. Express **29**, 6599 (2021).
23. P. Forster, C. Romano, J. Schneider, M. Eichhorn, and C. Kieleck, Opt. Lett. **47**, 2542 (2022).
24. N. Kishi and T. Yazaki, IEEE Photonics Technol. Lett. **11**, 182 (1999).
25. R. Poozesh, K. Madanipour, and P. Parvin, J. Lightwave Technol. **36**, 4880 (2018).
26. N. J. Ramírez-Martínez, M. Núñez-Velázquez, and J. K. Sahu, Opt. Express **28**, 24961 (2020).
27. S. Stepanov, M. P. Sanchez, and E. H. Hernández, J. Opt. Soc. Am. B **34**, 2089 (2017).
28. J. Zhang, Q. Sheng, L. Zhang, C. Shi, S. Sun, W. Shi, and J. Yao, Adv. Photonics Res. **3**, 2100256 (2022).
29. K. Zhang and J. U. Kang, Opt. Express **16**, 14173 (2008).
30. J. Zhang, Q. Sheng, L. Zhang, C. Shi, S. Sun, X. Bai, W. Shi, and J. Yao, Opt. Express **29**, 21409 (2021).
31. S. Melle, O. G. Calderón, Z. C. Zhuo, M. A. Antón, and F. Carreño, J. Opt. Soc. Am. B **28**, 1631 (2011).